

# Structure, electronic, optical and elastic properties of $(\text{NH}_4)_2\text{BeF}_4$ crystal in paraelectric phase

M.Ya. Rudysh<sup>a,b,c,d,\*</sup>, A.O. Fedorchuk<sup>e</sup>, V.Yo. Stadnyk<sup>a</sup>, P.A. Shchepanskyi<sup>a,b,d</sup>, R.S. Brezvin<sup>a</sup>, B.I. Horon<sup>a</sup>, O.Yu. Khyzhun<sup>f</sup>, O.M. Gorina<sup>d</sup>

<sup>a</sup> Physical Faculty, Ivan Franko National University of Lviv, 19 Dragomanov Str., UA-79005, Lviv, Ukraine

<sup>b</sup> Faculty of Science and Technology, J. Dlugosz University, 13/15 Armii Krajowej Al., PL-42-201, Czestochowa, Poland

<sup>c</sup> Educational and Scientific Physical and Technological Institute, Lesya Ukrainka Volyn National University, 9 Potapova Str., UA-43025, Lutsk, Ukraine

<sup>d</sup> Department of General Physics, Lviv Politechnic National University, 12 Bandery Str, UA-79013, Lviv, Ukraine

<sup>e</sup> Department of Inorganic and Organic Chemistry, Lviv National University of Veterinary Medicine and Biotechnologies, 50 Pekarska Str., UA-79005, Lviv, Ukraine

<sup>f</sup> Frantsevych Institute for Problems of Materials Science, National Academy of Sciences of Ukraine, 3 Krzhizhanovsky Str., UA-03142, Kyiv, Ukraine

## ARTICLE INFO

### Keywords:

Ammonium tetrafluoroberyllate  
Band structure  
Dielectric function  
Elastic properties  
Anisotropy  
Density functional theory

## ABSTRACT

The theoretical study of the structure and specific properties of the  $(\text{NH}_4)_2\text{BeF}_4$  crystal is carried out within the framework of the DFT. The band-energy structure of the  $(\text{NH}_4)_2\text{BeF}_4$  crystal in paraelectric phase is calculated and discussed. The edge of the fundamental absorption of the crystal is assumed to be associated with direct transitions in the center of Brillouin zone. The real and imaginary parts of the dielectric function as well as spectral dependence of the principal refractive indices of the crystal are calculated. Experimental study of the refractive indices dispersions of the grown crystal is carried out; the calculated dependences reveal good agreement with experimental data. Theoretical elastic coefficients  $C_{ij}$  are calculated. The anisotropy of optical and elastic properties, which is important for possible applications, has been highlighted by means of the 2D and 3D graphs. The presented results should be very useful for future anisotropy-based implementations of the crystal.

## 1. Introduction

Crystals which are transparent in the visible region of the spectrum are attractive objects of study for scientists due to their potential practical use in optical electronics devices. Transparency in a wide spectral range, mechanical stability, absence of phase transitions in the working area, and a high laser damage threshold are important characteristics of materials needed for their use in electromagnetic radiation modulators, laser technology, piezoelectric transducers, sensors, etc. An important class of materials which are transparent in the optical region of the spectrum are crystals belonging to the  $\text{A}_2\text{BX}_4$  group. Previously, some crystals of this group have been studied, and many of them were found to have a series of phase transitions that are accompanied by changes in crystal symmetry and, as a consequence, their physical properties [1–5]. The influence of structural transformation on the optical properties was studied for a row of  $\text{A}_2\text{BX}_4$  crystals like  $\text{K}_2\text{SO}_4$  [6],  $\text{LiNH}_4\text{SO}_4$  [7,8],  $\text{K}_{1.75}(\text{NH}_4)_{0.25}\text{SO}_4$  [9]. It was also shown a significant effect of isomorphous substitutions and impurities addition on the electronic structure

and optical parameters of  $\text{A}_2\text{BX}_4$  crystals [9–11] like in a case of some semiconductors [12,13]. The study of such an effect can be used for predicting new materials with predetermined properties.

A promising representative of the  $\text{A}_2\text{BX}_4$  group is ammonium tetrafluoroberyllate crystal (AFB),  $(\text{NH}_4)_2\text{BeF}_4$ . It can be grown from aqueous solution by temperature lowering method [14]. Structural studies of the crystal were conducted in Refs. [15–18]. AFB reveal three possible crystalline phases. At low temperatures, the crystal is in the ferroelectric phase with the  $Pcn2_1$  space group symmetry. At a temperature of  $T = 176$  K [16] there is a phase transition from the ferroelectric phase to incommensurate phase [15] with a modulation vector  $\mathbf{q} = 0.5 \mathbf{a}^*$  [19]. An incommensurate phase is observed up to  $T = 182$  K. At this temperature, the crystal began transition to the paraelectric phase with the  $Pm\bar{c}n$  space group symmetry.

Previously, reported were studies of uniaxial pressure on phase transitions and temperature-spectral-pressure dependences of the refractive properties of  $(\text{NH}_4)_2\text{BeF}_4$  crystal [20]. According to the spectral-temperature behavior of the refractive indices and

\* Corresponding author. Physical Faculty, Ivan Franko National University of Lviv, 19 Dragomanov Str., UA-79005, Lviv, Ukraine.

E-mail address: [rudysh.myron@gmail.com](mailto:rudysh.myron@gmail.com) (M.Ya. Rudysh).

<https://doi.org/10.1016/j.cap.2022.11.005>

Received 4 May 2022; Received in revised form 3 November 2022; Accepted 8 November 2022

Available online 12 November 2022

1567-1739/© 2022 Korean Physical Society. Published by Elsevier B.V. All rights reserved.

birefringence of ABF, there is a birefringence sign inversion (an isotropic point) in a crystal, which reveals isospectrality and can be controlled using uniaxial mechanical pressures. The phenomenon of isotropic point in AFB can be used in thermometry and pressure sensing [21], and for different types of electromagnetic radiation control devices [22,23].

Additionally  $(\text{NH}_4)_2\text{BeF}_4$  reveals good piezo-optical properties [24]. Spectroscopic studies of the AFB crystal doped with  $\text{Co}^{2+}$  have been reported in Ref. [25], and a consistent theoretical simulations of the absorption spectra using exchange charge model of crystal field have been performed.

Beside the considerable interest to the crystal, the fundamental study of the electronic structure of the AFB for room-temperature phase has not been reported in the literature, to the best of our knowledge. Only the band-structure study of the AFB crystal in the ferroelectric phase (low temperature phase) was performed so far [26]. Therefore, study of the electronic properties of FBA remains relevant. In particular, the interest in such a study is enforced by the possible peculiarities in the electronic spectrum of the crystal owing to the presence of light atoms in the structure, and fluorine. The latter can reveal strong chemical action and, as a consequence, significantly affect the properties of the material.

The work is devoted to the first-principles study of the electronic structure, optical spectra and elastic properties of FBA crystals, and experimental study of the spectral dependences of refractive indices at room temperature. The paper consists of three sections. The second section provides details of the synthesis and experimental studies, as well as a description of the methodology and parameters used for the calculations. The third section is devoted to the coverage of the results of calculations, their discussion and comparison with the experimental results. At the end of the article the main conclusions are made.

## 2. Methods of calculation and experimental technique

### 2.1. Crystal growing and refractive index measurements

The FBA crystals was grown from the aqueous solution using the temperature lowering method. Commercially available  $(\text{NH}_4)_2\text{BeF}_4$  salt of high purity (99.98%) was dissolved in the distilled water. The solution was filtrated, poured into the container and placed into the thermostat where crystallization was carried out. The saturated solution was cooled from 60 °C to 20 °C. The temperature decreasing was controlled by the microcontroller with precision  $\Delta T = 0.1$  °C. Obtained crystal revealed good optical quality and had a well-defined crystallographic shape with dimensions about  $38 \times 25 \times 18$  mm.

Measurements of the refractive indices  $n_i(\lambda)$  was performed using the standard immersion method with an accuracy not less than  $2 \times 10^{-4}$ . The method is well suited for the  $\text{A}_2\text{BX}_4$  crystals study and is described for instance in Refs. [7,8,10]. The refractive indices of studied crystals were measured on thin plates cut from large single crystal using diamond saw. Oriented plates with thickness approximately 0.1–0.2 mm and with parallel faces was polished using diamond paste. As immersion liquid the mixture of gasoline and isopropyl alcohol was used.

### 2.2. Computational details

Calculation of the electronic structure and physical properties of  $(\text{NH}_4)_2\text{BeF}_4$  crystal was performed using CASTEP program [27]. The program is based on the density functional theory (DFT) [28,29]. The method implemented in the program combines the pseudopotential approach together with the plane waves, which makes it fast and widely used in chemistry and solid-state physics. The ultrasoft pseudopotential was used for ionic core description. For the valence electrons, the following electronic configuration was used: H  $1s^1$ ; Be  $2s^2$ ; N  $2s^2 2p^3$ ; F  $2s^2 2p^5$ . The cut-off energy, which controls the number of plane waves was set at 400 eV. Integration over the 1st Brillouin zone was performed at points of the  $3 \times 3 \times 2$  k-mesh chosen by Monkhorst-Pack scheme [30]. The values of cut-off energy and k-mesh used for calculations were

obtained from preliminary test of total energy convergence. The solution of the Kohn-Sham equations is self-consistent in the method. The self-consistent procedure was performed until the preliminary set criterion of  $2 \times 10^{-7}$  eV was reached. The generalized gradient approximation (GGA) together with Perdew-Burke-Ernzerhof (PBE) parametrization were used for description of quantum effects of exchange and correlation [31]. The method is well tested on a row of isomorphic to AFB crystals of  $\text{A}_2\text{BX}_4$ -group, showing good agreement of calculated results with available experimental data (see e.g. Ref. [7]). The crystal structure was optimized before the calculations of electronic structure and physical properties. The Broyden-Flatcher-Goldfarb-Shanno algorithm (BFGS) was applied for optimization of the experimental structure [32]. The procedure was performed with the following convergence criterion: maximum force  $3 \times 10^{-2}$  eV/Å; maximum stress  $5 \times 10^{-3}$  GPa; maximum atomic displacement  $1 \times 10^{-4}$  Å.

## 3. Results and discussion

### 3.1. Crystal structure of $(\text{NH}_4)_2\text{BeF}_4$ crystals

First, let us consider the structural peculiarities of the close relative of AFB, the ammonium sulfate (AS) crystal, physical properties of which are far more studied. The crystalline structure of AS compound in the room-temperature phase  $[\text{NH}_4]_2[\text{SO}_4]$  rt, oP28,62 [33] is the same as in the low-temperature phase  $[\text{NH}_4]_2[\text{SO}_4]$  lt, oP36,33 [34] and can be represented as stacking of  $[\text{SO}_4]^{2-}$  (orange tetrahedra) and  $[\text{NH}_4]^+$  (blue tetrahedra) ions. Accordingly, the second coordination environment (SCE [35]) of anion atoms for these compounds are in the form of a hexagonal analogue of a cuboctahedron, as presented in Fig. 1. As can be seen from Fig. 1, the nearest coordination environment (NCE [36]) of anion atoms in both compounds is in the form of a deformed trigonal prism with one additional atom against the side face.

The structure of AFB compound,  $[\text{NH}_4]_2[\text{BeF}_4]$  rt, oP28,62 [17] or its split version  $[\text{NH}_4]_2[\text{BeF}_4]$ , oP76,62 [18] is represented by a similar second coordination environment and nearest coordination environment for anion atoms. During the temperature decreasing occurs the lowering of symmetry within identical space groups both in  $[\text{NH}_4]_2[\text{BeF}_4]$  lt, oP56,33 [17] and corresponding sulfate. As can be seen from the NCE of cation atoms within the SCE of anions of the  $[\text{NH}_4]_2[\text{BeF}_4]$  rt and  $[\text{NH}_4]_2[\text{SO}_4]$  rt crystals (Fig. 2), at almost identical ionic radiuses of  $\text{F}^-$  and  $\text{O}^{2-}$  the interatomic distances F–H are reduced compared to the corresponding O–H distances. This may indicate different conditions for the location of  $[\text{NH}_4]^+$  cations within the same type of anionic sublattices, that can be traced on the example of the studied physical properties of materials based on these compounds.

Before calculating the electronic parameters, such as density of states and band-energy structure, as well as other physical properties of the material, the obligatory geometric optimization of the structure was performed. In this work, we performed a complete geometric optimization, which includes the search for equilibrium lattice parameters and the coordinates of atoms that correspond to the ground state of the system. During the optimization procedure, the symmetry of the unit cell was constrained. The parameters of the crystal lattice of the ammonium fluoroberylate crystal obtained by geometric optimization are shown in Table 1. Here, for comparison, given is the experimental data of X-ray analysis taken from the literature [17].

As seen from Table 1, the optimized using the GGA functional crystal lattice parameters are close to the experimental ones. For the optimized geometry observed is overestimation of the lattice parameters, and as a result the increased cell volume. Previously, such overestimation was observed for the  $\text{LiNH}_4\text{SO}_4$  [7],  $\text{K}_2\text{SO}_4$  [37],  $\text{LiNaMo}_9\text{O}_{30}$  [38] crystals, and other, and can be referred to a general characteristics of GGA-based optimization. The *a* lattice parameter of the AFB crystal almost coincides with the experimental data (deviation is <1%). Parameters *b* and *c* show stronger deviation, 16% and 5%, respectively. This may indicate the

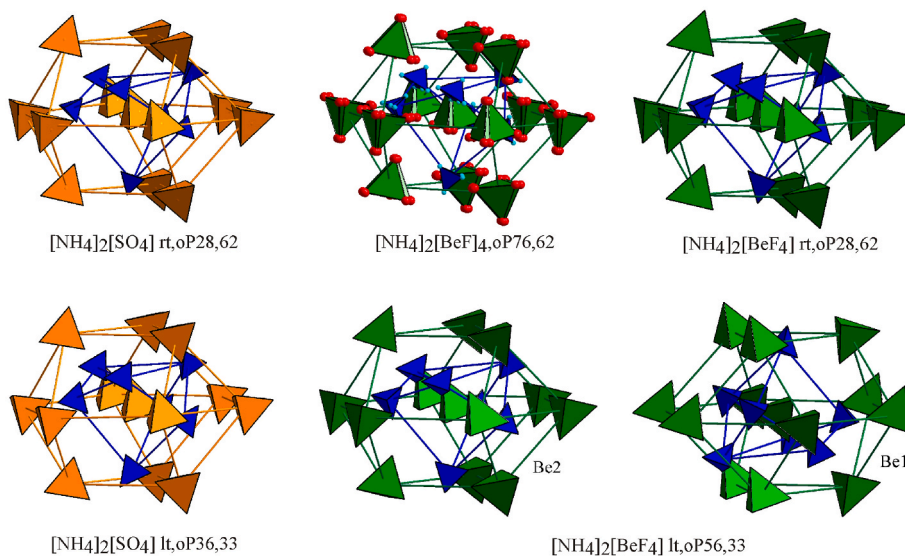


Fig. 1. Stacking of atoms within SCE in the structure of  $[\text{NH}_4]_2[\text{SO}_4]$  and  $[\text{NH}_4]_2[\text{BeF}_4]$  compounds.

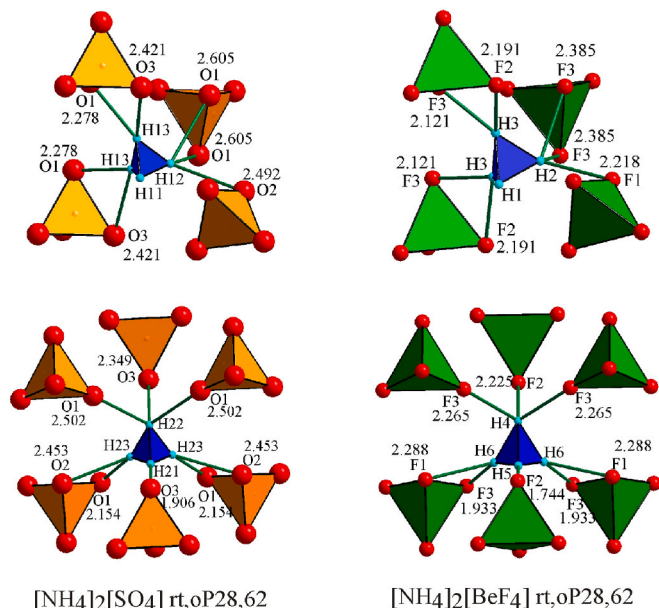


Fig. 2. The NCE of cation atoms within the SCE of anions in the structure of  $[\text{NH}_4]_2[\text{SO}_4]$  rt and  $[\text{NH}_4]_2[\text{BeF}_4]$  rt compounds.

Table 1

Experimental and optimized unit cell parameters of  $(\text{NH}_4)_2\text{BeF}_4$  crystal in the paraelectric phase.

Parameter	Experiment [17]	Calculation (GGA)
Space group no.	62	62
a, Å	7.531	7.587
b, Å	5.874	6.830
c, Å	10.399	10.941
V, Å <sup>3</sup>	460.02	566.95
Z	4	4

strong interaction between ions in direction of *a*-parameter, while the weakest bonding is in the direction of *b*-parameter, leading to unit cell deformation in the corresponding direction. The general deviation of the lattice volume of the optimized crystal structure is 23%.

### 3.2. Electronic structure

Electronic band structure defines majority of physical processes in materials. Its study is useful for explanation and interpretation of the already obtained experimental results of AFB. For the calculation of the band structure the optimized structural parameters of the crystal were taken as initial data. The band structure of  $(\text{NH}_4)_2\text{BeF}_4$  was calculated at the high-symmetry points of Brillouin zone and along the lines that connect them in the following direction:  $\Gamma \rightarrow Z \rightarrow T \rightarrow Y \rightarrow S \rightarrow X \rightarrow U \rightarrow R$ . The electronic band structure of  $(\text{NH}_4)_2\text{BeF}_4$  crystal calculated with GGA functional is shown in Fig. 3. The structure of the first Brillouin zone is depicted on insert of Fig. 3. The band structure is built in the energy range from  $-22$  eV to  $15$  eV and this range can be divided into two regions. The valence band consists of a set of narrow bands located near  $-20$  eV,  $-16$  eV,  $-5$  eV and in the energy range from  $0$  to  $-3$  eV. These bands become wider with the approaching of the top of valence band. The topmost band is the widest in the valence band. All levels of the valence band are nearly flat. Considering the low dispersion of levels, it can be concluded that the top of valence band is located at  $\Gamma$

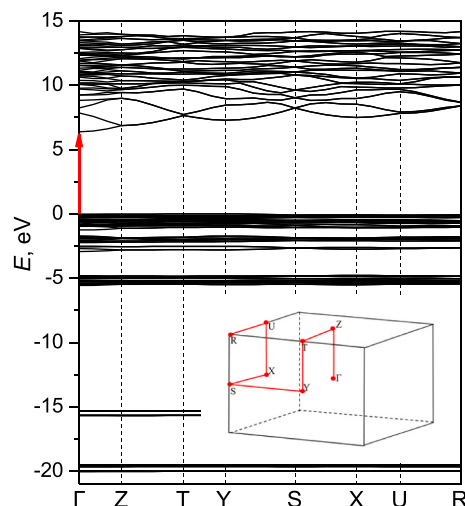


Fig. 3. Calculated band structure of  $(\text{NH}_4)_2\text{BeF}_4$  crystal. The structure of Brillouin zone for orthorhombic crystal is shown on insert. The coordinates of high-symmetry points are following:  $\Gamma$  (0; 0; 0); Z (0; 0; 0.5); T (-0.5; 0; 0.5); Y (-0.5; 0; 0); S (-0.5; 0.5; 0); X (0; 0.5; 0); U (0; 0.5; 0.5); R (-0.5; 0.5; 0.5).

point of Brillouin zone. A low dispersion of energy levels was previously shown for other crystals of  $A_2BX_4$  like  $LiNH_4SO_4$  ( $\alpha$ - and  $\beta$ -modifications),  $LiNaSO_4$ ,  $K_{1.75}(NH_4)_{0.25}SO_4$ ,  $K_2SO_4$ , etc. and is related to quite significant isolation of structural complexes in crystals, which for the case of AFB crystal are the  $NH_4$  and  $BeF_4$  tetrahedra. Particularly, it can be explained by the fact, that the atoms inside the  $NH_4$  and  $BeF_4$  complexes are bonded by strong covalent bonds, and hence, the corresponding tetrahedra interact by ionic bond.

Conduction band of the crystal consists of a wide band from 6.3 eV to 14 eV and is characterized by the significant dispersion of four lowest energy levels. Electron levels at higher than 10 eV energies reveal a low dispersion similarly to the valence-band's levels. The bottom of conduction band is located at the center of Brillouin zone. Therefore, one can conclude, that fundamental edge of the crystal is formed by the direct  $\Gamma_v \rightarrow \Gamma_c$  electronic transitions. The band gap value estimated from the calculated with the GGA functional band structure is equal to 6.39 eV. Unfortunately, the experimental fundamental absorption edge study, from which the exact band gap value can be obtained is unknown by now. It is a known fact that when calculating the band-energy structure within the formalism of the density functional theory with using GGA functional, the band gap is underestimated [38,39]. This underestimation, as reported in the literature, can reach 50% of the true value obtained from the experiment. In some cases, for narrow-band semiconductors, it may erroneously give a zero value of  $E_g$ . In Ref. [8], the band-energy structure of  $\beta$ - $LiNH_4SO_4$  crystal was studied and it was estimated that values of the band-gap underestimation for materials of  $A_2BX_4$  group are near 2 eV. Therefore, we predict that the band gap value  $E_g$  for  $(NH_4)_2BeF_4$  crystal should be close to 8 eV. Any other theoretical studies of the  $(NH_4)_2BeF_4$  crystal at room temperature (paraelectric phase) are absent in the literature, however, previously calculations were performed for the AFB crystal in the ferroelectric phase. For the low-temperature phase of the crystal, calculated using the same approach band gap value is  $E_g = 6.79$  eV [26]. It follows that as the temperature increases and transition from the ferroelectric phase to the paraelectric phase through the incommensurate phase takes place, the band gap of the crystal increases.

In general, the band structure of  $(NH_4)_2BeF_4$  crystal is very similar to that of studied recently sulfate-group crystals. Here, the theoretical studies of  $LiNH_4SO_4$  [8],  $LiNaSO_4$  [40],  $K_{1.17}[NH_4]_{0.25}SO_4$  [9], and other crystals of  $ABSO_4$  group showed similar flatness of valence bands. The lowest levels of conduction bands of these crystals also reveal the highest dispersions with the conduction band bottom located at  $\Gamma$  point. The previous experimental study of XPS and XES spectra for  $LiNH_4SO_4$  in  $\alpha$ - [7] and  $\beta$ - [8] modifications, and  $K_2SO_4$  [10] crystal showed perfect agreement of experimental spectra with the calculated using GGA functional band structures and spectra of partial density of states, confirming the high suitability of the applied method for study of such materials. The band structure of the isostructural to AFB  $(NH_4)_2SO_4$  crystal has quite similar dispersion, but the band gap is of indirect type. The lowest calculated bandgap value for ammonium sulfate crystal is equal to 4.6 eV, being 1.79 eV smaller than for  $(NH_4)_2BeF_4$  crystal. Therefore, the increasing of band gap value at substitution  $SO_4 \rightarrow BeF_4$  is observed.

Calculated using GGA functional total density of states (DOS) and partial density of states (PDOS) are depicted in Fig. 4. The main peak for N atom in the PDOS spectra is located at  $-5$  eV and corresponds to  $2p$ -electrons. Near  $-15$  eV  $2s$ -states of nitrogen are represented by the peak of low intensity.  $1s$ -states of H are presented in the valence band at  $-5$  eV and  $-16$  eV, hybridized with the nitrogen states. The main contribution of hydrogen atoms is in the conduction band. The main contribution of beryllium atoms is represented by the  $2s$  states in the bottom of the conduction band. The F- $2s$  states are presented in the spectrum at  $-20$  eV by the intensive peak. The F- $2p$  states form the highest valence levels. As evidenced from the PDOS spectra the fundamental absorption edge of  $(NH_4)_2BeF_4$  crystal is likely to be formed by the transition from the F- $2p$  states to  $2s$ -states of beryllium.

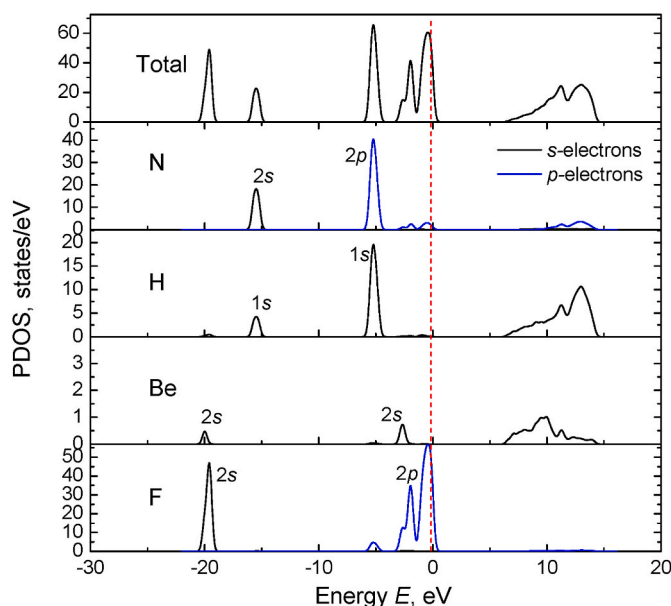


Fig. 4. DOS and PDOS of  $(NH_4)_2BeF_4$  crystal calculated using GGA functional.

As additional study of the electronic properties of AFB, Mulliken and bond population charges were calculated. This allows to obtain useful information on chemical bonding, which can be extracted from the atomic charges and bond population analysis using the Mulliken formalism. The calculation of charges is based on the method of linear combination of atomic orbitals (LCAO), and the implementation of this method was carried out by Segall et al. [41,42]. The atomic populations for  $(NH_4)_2BeF_4$  crystal were calculated using the GGA functional and are collected in Table 2. Deviation of the effective charges in crystal from ones expected from the chemical formula can testify about dominating covalent character of the chemical bonding and strong hybridization of bonds in  $(NH_4)_2BeF_4$  crystal.

The shortest cation-anion distances for the constituent atoms of the  $(NH_4)_2BeF_4$  compound together with bond overlap populations calculated using GGA functional are collected in Table 3. The maximum population of N — H bond in AFB is 0.62. At the same time, Be — F bonds has population 0.31. To additionally analyze the type of bonding, we calculated the ionicity of bonds using the following equation

$$f_h = 1 - e^{-\frac{|P_c - P|}{P}}, \quad (1)$$

here  $P$  is overlap population, and  $P_c$  is overlap population of purely covalent crystal and is equal to 1. The equality of the  $f_h$  parameter to 1 indicates an ionic bonding type, while zero value indicates a pure covalent bonding type. The calculated values of the bonds ionicity are also given in Table 3. As can be seen from the table, the crystal has a covalent-ionic type of chemical bonding with a large contribution of ionic component. Atoms in the  $[NH_4]$  and  $[BeF_4]$  structural complexes are joined by covalent bonding, although  $[BeF_4]$  tetrahedra reveal a high degree of ionic component in Be — F bonding. The  $[BeF_4]$  and  $[NH_4]$  complexes interact with each other by the ionic bonds.

Similar conclusions can be drawn from the consideration of

Table 2

Atomic populations (by Mulliken) (in units of the proton charge) of the constituent atoms of  $(NH_4)_2BeF_4$  crystal.

Species	s	p	d	Total	Charge (e)
H	0.58	0.00	0.00	0.58	0.42
Be	0.17	0.56	0.00	0.72	1.28
N	1.66	4.36	0.00	6.01	-1.01
F	1.95	5.71	0.00	7.66	-0.66

**Table 3**

Lengths and overlap populations of the shortest atomic bonds and bond ionicity of  $(\text{NH}_4)_2\text{BeF}_4$  crystal.

Bond	Population	Length (Å)	$f_h$
H – N	0.62	1.04759	0.46
Be – F	0.31	1.60791	0.89

electronegativity of atoms. For the  $\text{NH}_4$  tetrahedra the difference in the electronegativities of the N and H atoms is equal  $\Delta\chi = 0.9$ . A small value of electronegativity difference indicates a significant fraction of covalency in the N – H chemical bond in the corresponding tetrahedra. For  $\text{BeF}_4$  complexes the electronegativity difference between the Be and F atoms is  $\Delta\chi = 2.5$ , that is usual for bonds with the significant fraction of ionicity. The consideration of the chemical bond character shows the agreement between the calculation of bond populations and electronegativity differences analysis.

For clarity, we calculated the charge distribution near the corresponding structural units. Fig. 5 shows the charge density cross-section along the N – H and Be – F bonds. As one can see, the distribution of the electronic charge in  $\text{NH}_4$  tetrahedra is characterized by the deformation together with the strong overlapping of electronic clouds of N and H atoms, respectively. Such distribution is typical for directed covalent type of chemical bond. In  $\text{BeF}_4$  tetrahedra charge density is of spherical shape, confirming almost purely ionic bonding between the F and Be atoms. This fact is in consistency with the results of the bond charge population analysis and analysis of the electronegativities.

### 3.3. Optical spectra

AFB is known to be a transparent dielectric crystal [20]. According to the symmetry, the crystal is biaxial and its optical indicatrix is characterized by three different refractive indices. Unfortunately, experimental studies of AFB in a wide spectral range are lacking in the literature, thus theoretical study of optical spectra are performed in this work.

Optical properties of solids can be described by dielectric function  $\varepsilon(\omega)$ , which is the complex function  $\varepsilon(\omega) = \varepsilon_1(\omega) + i\varepsilon_2(\omega)$ , where  $\varepsilon_1(\omega)$  and  $\varepsilon_2(\omega)$  are real and imaginary parts of dielectric function, respectively. This function is related with other optical functions, like refractive index  $n(\omega)$ , extinction coefficient  $k(\omega)$ , absorption coefficient  $\alpha(\omega)$ , optical conductivity  $\sigma(\omega)$ , etc. The absorption processes are associated with the imaginary part of dielectric function  $\varepsilon_2(\omega)$  [43]. The latter can be estimated by integration of elements of dipole matrix operator between the filled states of valence band and empty levels of conduction band

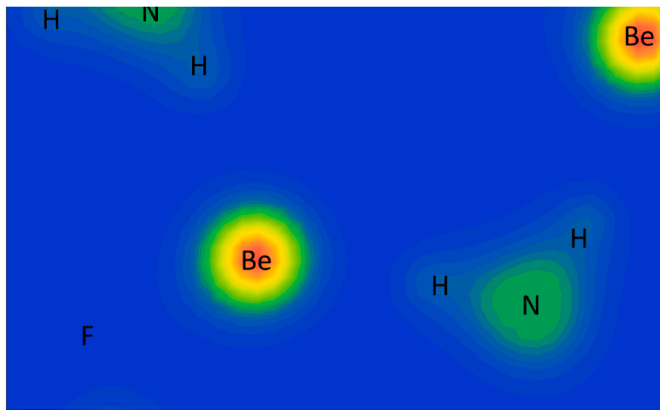


**Fig. 5.** Cross-sections of charge density for N – H and Be – F bonds of the  $(\text{NH}_4)_2\text{BeF}_4$  crystal calculated using GGA functional.

$$\varepsilon_2(\omega) = \frac{2\pi e^2}{\Omega \varepsilon_0} \sum_{k,v,c} |\langle \psi_k^c | \mathbf{ur} | \psi_k^v \rangle|^2 \delta(E_k^c - E_k^v - E), \quad (2)$$

where  $e$  is the electron charge,  $\Omega$  is the unit cell volume;  $\psi_k^c$  and  $\psi_k^v$  are the wave functions of the conduction band and valence band in  $k$ -space, respectively;  $\varepsilon_0$  is the dielectric permittivity of vacuum;  $\mathbf{u}$  is the incident photon polarization vector;  $\mathbf{r}$  is the operator of electron position, and  $E$  is the photon energy. The real part of the dielectric function  $\varepsilon_1(\omega)$  is related to its imaginary part  $\varepsilon_2(\omega)$  and can be obtained from it using the Kramers–Kronig relation [44]

$$\varepsilon_1(\omega) = 1 + \frac{2}{\pi} \int_0^\infty \frac{\varepsilon_2(\omega') \omega' d\omega'}{\omega'^2 - \omega^2}. \quad (3)$$

Due to anisotropy of crystalline materials the dielectric function describing it is a tensor quantity. According to the symmetry of  $(\text{NH}_4)_2\text{BeF}_4$ , the crystal should be characterized by three different  $\varepsilon_x$ ,  $\varepsilon_y$ , and  $\varepsilon_z$  values. Fig. 6 shows the dielectric functions of the  $(\text{NH}_4)_2\text{BeF}_4$  crystal calculated in this work for polarized light and for the 0–35 eV energy range. As one can see, the dielectric function possesses a significant anisotropy. Its values are close for  $X$  and  $Z$  directions in the low-energy range and for the  $Y$  and  $Z$  directions at higher energies. The static dielectric constant ( $\omega \rightarrow 0$ ) obeys the following inequality  $\varepsilon_x > \varepsilon_z > \varepsilon_y$  and is equal to  $\varepsilon_x = 1.255$ ,  $\varepsilon_y = 1.236$ , and  $\varepsilon_z = 1.250$ . The main peak in the imaginary dielectric function  $\varepsilon_2(\omega)$  referred to the transition of the electron from the top of the valence band to the bottom of the conduction band when absorbing a quantum of light with energy corresponding to the band gap is located at the energy of  $\sim 7.9$  eV. It corresponds to  $\Gamma_v \rightarrow \Gamma_c$  transition. This peculiarity is marked as  $a$  on  $\varepsilon_2(\omega)$  spectra (Fig. 6 b). By analyzing the band structure, one can conclude, that low-frequency peaks denoted as  $a$  and  $b$  correspond to  $2p \rightarrow 2s$  electron transition between fluorine and beryllium atoms, respectively. The  $c$  and  $d$  peculiarities that contributes to  $\varepsilon_2(\omega)$  spectra at higher energies correspond to the  $2p \rightarrow 1s$  electron transitions from nitrogen to hydrogen atoms inside the  $\text{NH}_4$  tetrahedra, respectively. According to this, one can conclude that the  $\text{BeF}_4$  complexes give main contribution to  $\varepsilon_2(\omega)$  in the low-energy range of the spectrum. The results obtained for AFB crystal at room temperature are pretty close to the results obtained by us for ferroelectric phase of AFB crystal at low temperature [26].

Using the equation

$$n(\omega) = \sqrt{\frac{(\varepsilon_1(\omega)^2 + \varepsilon_2(\omega)^2)^{1/2} + \varepsilon_1(\omega)}{2}}, \quad (4)$$

the values of refractive indices  $n$  can be obtained from the spectra of the dielectric function. Fig. 7 shows the spectral dependence of the refractive indices  $n(\omega)$  in the spectral range from 200 to 800 nm. The refractive indices of the crystal obey the following sequence  $n_z > n_x > n_y$  in this spectral region and the dispersion of refractive indices is normal ( $dn_i/d\lambda < 0$ , for  $i = X, Y$ , and  $Z$ ). The refractive indices for  $X$  and  $Z$  directions are close to each other and reveal almost the same dispersion in all spectral range. Such a characteristic can indicate possibility to induce a birefringence sign inversion or isospectrality in the crystal by the temperature changing, applying of stresses or electric field.

In order to confirm these results, we have grown the  $(\text{NH}_4)_2\text{BeF}_4$  crystal and performed the refractive index measurements. Photograph of the large single crystal obtained (approximately  $38 \times 25 \times 18$  mm in size) is presented on the insert of Fig. 7. The crystal was homogenous and of a good optical quality. The experimental results on the refractive indices for FBA crystal at room temperature are also depicted in Fig. 7. It can be seen from the figure, that the refractive indices  $n_x \approx n_z$ , and in the spectral range from 200 to 800 nm  $n_z$  is a bit smaller than the refractive index in  $X$  direction. These results are in good agreement with the theoretically calculated data. The experimental data shows that the refractive indices from the calculations are underestimated. This

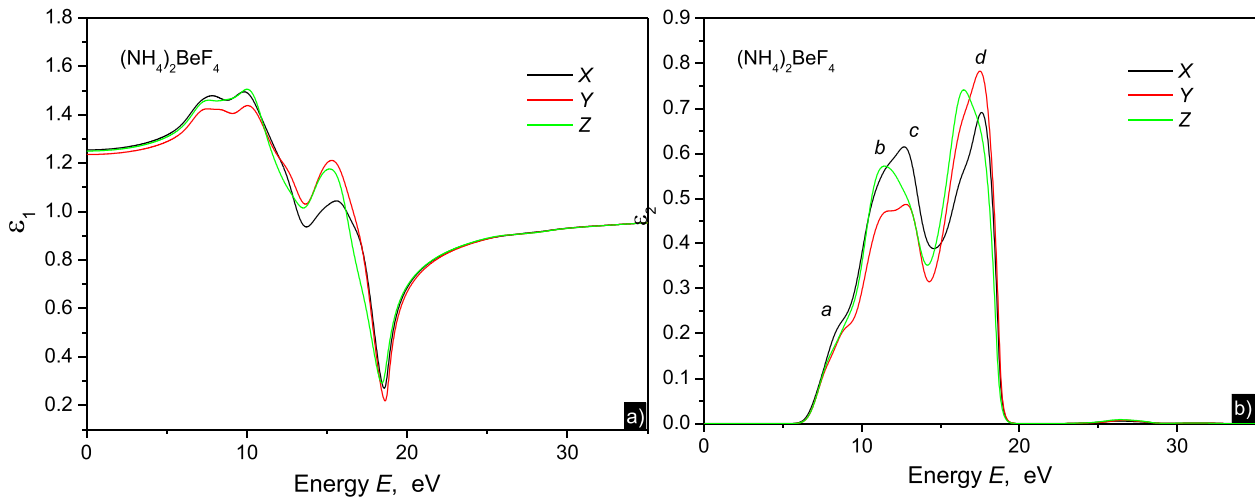


Fig. 6. Real and imaginary parts of dielectric functions of  $(\text{NH}_4)_2\text{BeF}_4$  crystal calculated using GGA functional.

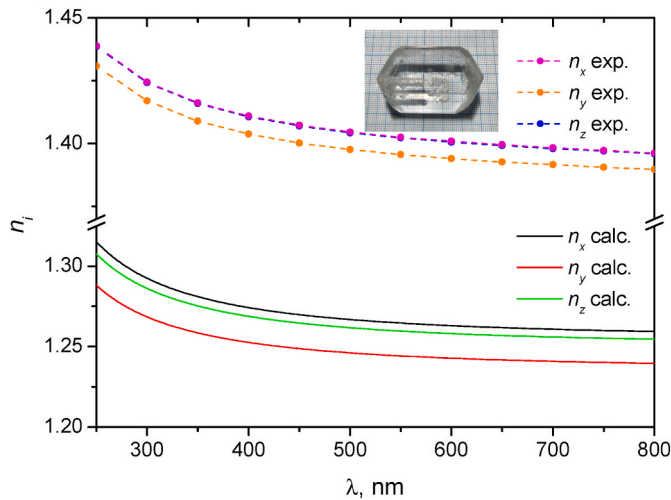


Fig. 7. Calculated and experimental refractive indices for  $(\text{NH}_4)_2\text{BeF}_4$  crystal.

underestimation can be caused by the disregard in current calculations of indirect optical transitions, frozen phonons, as well as absence of quasiparticles like excitons etc.

### 3.4. Elastic properties

State-of-the-art methods based on DFT allow not only electronic-structure and optical properties calculations. Possible is also to obtain elastic properties of solids, which are of a great interest from both a fundamental and applied point of view. Elastic properties are related with the sound velocities, heat transport, microcracks etc. In general, elastic properties can be characterized by Hooke's law, which for anisotropic materials has the following form

$$\sigma_{ij} = C_{ijkl} \varepsilon_{kl} \quad (5)$$

where  $\sigma_{ij}$  is mechanical stress tensor,  $C_{ijkl}$  the elastic coefficients,  $\varepsilon_{kl}$  the deformation tensor. As a result of convolution only 36 components from total 81 components remain. Since the  $(\text{NH}_4)_2\text{BeF}_4$  belongs to the orthorhombic symmetry class, the linear elastic coefficients form a  $6 \times 6$  symmetric matrix having 12 non-zero components for orthorhombic phase, which than can be reduced to nine independent components ( $C_{11}$ ,  $C_{22}$ ,  $C_{33}$ ,  $C_{44}$ ,  $C_{55}$ ,  $C_{66}$ ,  $C_{12}$ ,  $C_{13}$ , and  $C_{23}$ ).

The  $C_{ij}$  coefficients for the  $(\text{NH}_4)_2\text{BeF}_4$  crystal are obtained in this

work from the Taylor series decomposition of the total energy  $E(V, \delta)$  of the investigated system with respect to the unit cell volume  $V$ , similarly as was done in Refs. [39,45] using the expression

$$E(V, \delta) = E(V_0, 0) + V_0 \left( \sum_i \tau_i \xi_i \delta_i + \frac{1}{2} \sum_{ij} C_{ij} \delta_i \xi_i \delta_j \xi_j \right) + O(\delta^3), \quad (6)$$

where  $E(V_0, 0)$  is the energy of the unstrained system,  $V_0$  is the equilibrium volume,  $\tau_i$  is an element of the stress tensor, and  $\xi_i$  is the Voigt index [45]. The calculated elastic coefficients  $C_{ij}$  obtained for AFB crystal using GGA functional are given in Table 4. Born criterion was used to test the mechanical stability of the crystal structure [46]:

$$\begin{aligned} &C_{11} > 0, C_{22} > 0, C_{33} > 0, C_{44} > 0, C_{55} > 0, C_{66} > 0 \\ &[C_{11} + C_{22} + C_{33} + 2(C_{12} + C_{13} + C_{23})] > 0 \\ &(C_{11} + C_{12} - 2C_{12}) > 0 \\ &(C_{11} + C_{33} - 2C_{13}) > 0 \\ &(C_{22} + C_{33} - 2C_{23}) > 0 \end{aligned} \quad (7)$$

By inspecting Table 4, one can see that the elastic coefficients satisfy Born criterion (7). It means that the crystal is mechanically stable. The low values of the elastic coefficients indicate that  $(\text{NH}_4)_2\text{BeF}_4$  crystal is relatively mechanically soft. The maximum elastic coefficients component is  $C_{33} = 55.9$  GPa, while the lowest one is  $C_{66} = 5.11$  GPa. The main elastic coefficients form the following row  $C_{33} > C_{11} > C_{22}$ . As one can see, the shear components are significantly smaller than the compressional.

The experimental study of the elastic properties of AFB was reported by A. Garg et al. [47]. In Table 4 the experimental elastic coefficients of  $(\text{NH}_4)_2\text{BeF}_4$  crystal are shown for comparison. As one can see, both sets of data are quite similar showing a good agreement between the calculated  $C_{ij}$  values and reported previously data. Table 4 depicts also the corresponding calculated and experimental elastic coefficients of isostructural  $(\text{NH}_4)_2\text{SO}_4$ , given for comparison.

Elastic compliance matrix is related with elastic coefficients matrix as  $C_{ij} = S_{ij}^{-1}$ . The calculated and reported earlier experimental elastic compliance components are listed in Table 5.

The Young's moduli  $E_x$ ,  $E_y$  and  $E_z$  can be obtained from elastic compliance coefficients  $S_{ij}$  using following relations:  $E_x = S_{11}^{-1}$ ,  $E_y = S_{22}^{-1}$ ,  $E_z = S_{33}^{-1}$ . Poisson's ratios can be calculated as  $\nu_{ij} = S_{ij}/S_{ii}$ . The obtained characteristics for AFB are given in Table 6.

In order to characterize the elastic properties of polycrystalline material, the elastic modulus is often used. For this purpose, the bulk modulus  $B$  and shear modulus  $G$  should be calculated. Generally, those moduli are estimated from the Voigt-Reuss-Hill (VRH) model. The Voigt and Reuss scheme define respectively the maximum and minimum

**Table 4**  
Elastic coefficients  $C_{ij}$  (in GPa) of  $(\text{NH}_4)_2\text{BeF}_4$  crystal calculated using GGA functional.

	Method	$C_{11}$	$C_{22}$	$C_{33}$	$C_{44}$	$C_{55}$	$C_{66}$	$C_{12}$	$C_{13}$	$C_{23}$
$(\text{NH}_4)_2\text{BeF}_4$	GGA	36.8	39.4	55.9	6.2	7.6	5.1	10.1	22.5	19.3
$(\text{NH}_4)_2\text{BeF}_4$	Exp. <sup>a</sup>	38.2	35.6	24.5	9.6	10.1	7.9	17.8	15.2	14.1
$(\text{NH}_4)_2\text{SO}_4$	GGA <sup>b</sup>	43.9	50.8	28.0	2.7	3.4	7.4	18.4	11.1	15.1
$(\text{NH}_4)_2\text{SO}_4$	Exp. <sup>c</sup>	35.2	29.7	36.0	9.5	7.0	10.3	14.1	15.7	17.3

<sup>a</sup> Ref. [47].

<sup>b</sup> Ref [48].

<sup>c</sup> Ref [49].

**Table 5**  
Elastic compliance coefficients  $S_{ij}$  (in  $\text{GPa}^{-1}$ ) of  $(\text{NH}_4)_2\text{BeF}_4$  crystal calculated using GGA functional.

Method	$S_{11}$	$S_{22}$	$S_{33}$	$S_{44}$	$S_{55}$	$S_{66}$	$S_{12}$	$S_{13}$	$S_{23}$
GGA	0.0362	0.0308	0.0267	0.1622	0.1320	0.1957	−0.0026	−0.0136	−0.0096
Exp. <sup>a</sup>	0.0390	0.0410	0.0600	0.1040	0.0990	0.1270	−0.0130	−0.0170	−0.0150

<sup>a</sup> Ref. [47].

**Table 6**  
Young modulus  $E_i$  ( $i = x, y,$  and  $z$ ) (in GPa) and Poisson’s ratios  $\nu_{ij}$  ( $i, j = x, y, z$ ) calculated for  $(\text{NH}_4)_2\text{BeF}_4$  crystals using GGA functional.

$i$	$E_i$	$\nu_{ij}$			
$x$	27.62	$\nu_{xy}$	0.071	$\nu_{xz}$	0.377
$y$	32.51	$\nu_{yx}$	0.084	$\nu_{yz}$	0.312
$z$	37.47	$\nu_{zx}$	0.511	$\nu_{zy}$	0.360

limits of these moduli. In Table 7 the bulk moduli  $B$  and shear moduli  $G$  received by Voigt and Reuss schemes are given. The available experimental data is shown for the comparison. The Hill values are arithmetic mean of Voigt and Reuss values. The calculated  $B_V, B_R, B_H$  and  $G_V, G_R, G_H$  are in good agreement with the literature data.

The Pugh’s ratio  $B_H/G_H$  reflects the brittleness or ductility of a material and its critical value is 1.75. If Pugh’s ratio is larger than 1.75, the material is ductile; otherwise, it is brittle. Calculated for  $(\text{NH}_4)_2\text{BeF}_4$  crystal ratio is  $B_H/G_H = 2.97$ , indicating that the crystal is ductile.

In order to evaluate the degree of anisotropy of the material’s elastic properties, the anisotropy factors  $A_1, A_2, A_3$ , universal anisotropy index  $A^U$ , as well as bulk  $A_B$  and shear  $A_G$  anisotropy indices were calculated. The shear anisotropic factor for the (100) shear planes between the [011] and [010] directions is

$$A_1 = \frac{4C_{44}}{C_{11} + C_{33} - 2C_{13}}, \tag{8}$$

for the (010) shear planes between the [101] and [001] directions is

$$A_2 = \frac{4C_{55}}{C_{22} + C_{33} - 2C_{23}}, \tag{9}$$

and for the (001) shear planes between the [110] and [010] directions is

$$A_3 = \frac{4C_{66}}{C_{11} + C_{22} - 2C_{12}}. \tag{10}$$

The values of  $A_1, A_2,$  and  $A_3$  for an isotropic structure are equal to one, and their deviation from unity is a measure of the degree of me-

$$E = [S_{11}l_1^4 + 2S_{12}l_1^2l_2^2 + S_{22}l_2^4 + 2S_{23}l_2^2l_3^2 + S_{33}l_3^4 + 2S_{13}l_1^2l_3^2 + S_{44}l_2^2l_3^2 + S_{55}l_1^2l_3^2 + S_{66}l_1^2l_2^2]^{-1}, \tag{14}$$

chanical properties anisotropy. The calculated values of anisotropy factors for  $(\text{NH}_4)_2\text{BeF}_4$  crystal are  $A_1 = 0.514, A_2 = 0.535,$  and  $A_3 = 0.365$ . Therefore, the shear anisotropy in the (100) and (010) shear

**Table 7**  
Elastic bulk  $B$  and shear modulus  $G$  for polycrystalline  $(\text{NH}_4)_2\text{BeF}_4$  (in GPa) and experimental data for comparison.

Parameter	Voigt		Reuss		Hill	
	Calc.	Exp.	Calc.	Exp.	Calc.	Exp.
$B$	26.20	21.40	23.81	20.2	25.00	20.8
$G$	9.12	9.50	7.70	9.0	8.41	9.3

planes is almost the same in the crystal. The lower  $A_3$  value shows stronger deviation and higher anisotropy in (001) plane.

The bulk  $A_B$  and shear  $A_G$  anisotropy indices can be calculated using the following equations

$$A_B = \frac{B_V - B_R}{B_V + B_R} \times 100\%, A_G = \frac{G_V - G_R}{G_V + G_R} \times 100\%. \tag{11}$$

Here,  $A_B$  and  $A_G$  are equal to 0 for isotropic material, while for highly anisotropic material these values can increase up to near 100%. For  $(\text{NH}_4)_2\text{BeF}_4$  anisotropy indices  $A_B = 4.8\%$  and  $A_G = 8.4\%$ , indicating that the shear anisotropy is greater than the bulk anisotropy. The universal anisotropy index taking into account both the shear and bulk anisotropy can be calculated as

$$A^U = 5 \frac{G_V}{G_R} + \frac{B_V}{B_R} - 6. \tag{12}$$

The calculated value of  $A^U = 1.02051$  for  $(\text{NH}_4)_2\text{BeF}_4$  indicates significant anisotropy of elastic properties of this material.

The additional straightforward method to depict the anisotropy of the material’s elastic properties is to plot 3D surfaces of Young’s and bulk modulus. Young’s modulus and bulk modulus for the orthorhombic material can be obtained from the following equations

$$B = [(S_{11} + S_{12} + S_{13})l_1^2 + (S_{12} + S_{22} + S_{23})l_2^2 + (S_{12} + S_{23} + S_{33})l_3^2]^{-1}, \tag{13}$$

where  $S_{ij}$  is the elastic compliance,  $l_1, l_2,$  and  $l_3$  are the directional cosines. The spatial distribution of the Young’s modulus and bulk modulus for AFB is shown in Fig. 8. As one can see, the Young’s modulus has a

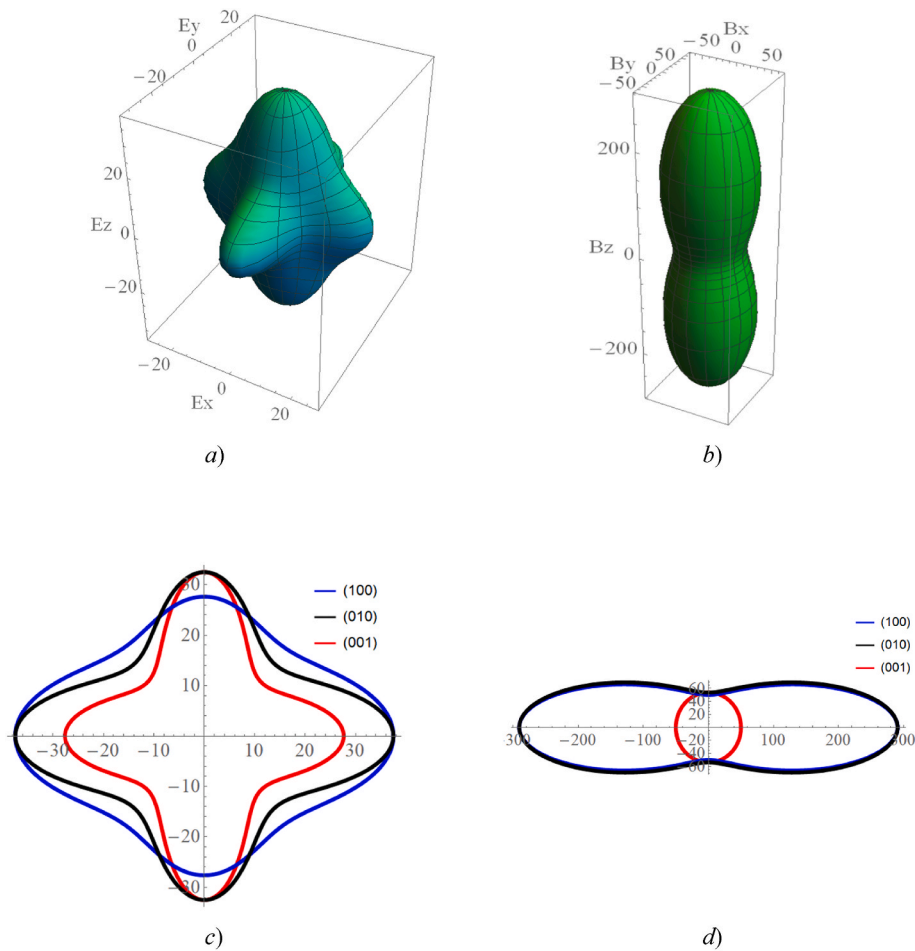


**Fig. 8.** 3D surface representation of the Young's modulus  $E$  (a), and bulk modulus  $B$  (b), and planar projections of the (100), (010) and (001) planes of the Young's modulus  $E$  (c) and Bulk modulus  $B$  (d) of  $(\text{NH}_4)_2\text{BeF}_4$  crystal plotted for the GGA-calculated elastic compliance.

significant anisotropy, which is higher than bulk modulus' anisotropy. The planar projections of the Young's modulus have a flower-like shape. One can see, that the Young's modulus in the (001) plane has greater anisotropy than in (100) and (010) planes. It is easy to see from the planar projections that (100) and (010) planes projections are almost identical and possess large anisotropy. At the same time, bulk modulus in (001) plane has a smaller value than in two other planes and has a shape of circle conforming the isotropic behavior of bulk modulus.

#### 4. Conclusions

Theoretical study of the band-energy structure of  $(\text{NH}_4)_2\text{BeF}_4$  crystal in paraelectric phase was performed in the present work using first-principles calculations within the framework of density functional theory for the first time. Ammonium fluoroberyllate crystal was found to be a direct-bandgap dielectric crystal with a band gap located at point  $\Gamma$ . The calculated band gap value is 6.39 eV. It was found that the replacement of structural complexes  $[\text{SO}_4]$  with  $[\text{BeF}_4]$  leads to an increase in the value of band gap obtained using GGA method by 1.79 eV. The origin of the energy bands in the crystal was determined from the calculation of the partial density of electronic states. It was found that the top of the valence band is formed by  $2p$  states of fluorine, while the bottom of the conduction band is formed by  $2s$  states of beryllium. Thus, the edge of fundamental absorption of the crystal should be formed by  $\text{F-}2p \rightarrow \text{Be-}2s$  transition, which occurs inside the  $\text{BeF}_4$  tetrahedra.

As seen from the Milliken charges and bonds population of the crystal, bonds inside the  $\text{NH}_4$  and  $\text{BeF}_4$  complexes are covalent with an ionic fraction. The  $\text{Be} - \text{F}$  bond reveals higher ionicity than  $\text{N} - \text{H}$

bond. These statements are further confirmed by the calculated electron density distribution and electronegativities analysis.

The calculated optical functions for the crystal show a significant anisotropy. The static dielectric constant ( $\omega \rightarrow 0$ ) obeys the following inequality  $\epsilon_x > \epsilon_z > \epsilon_y$  and is equal to  $\epsilon_x = 1.255$ ,  $\epsilon_y = 1.236$ , and  $\epsilon_z = 1.250$ . It is shown that the real part of the dielectric function and refractive indices in the optical region of the spectrum in the  $X$  and  $Z$  directions are close to each other, and the birefringence sign inversion or isospectrality of the crystal can be expected to be induced by temperature, stress, or electric field. The experimental study of the spectral dependence of refractive indices for grown AFB crystal was performed. The calculated values of refractive indices were found to be smaller than the experimental ones, yet the position of the dispersion curves agree with the experimental and dispersive changes are quantitatively close for both the calculated and experimental results.

The elastic coefficients and elastic compliance matrix were obtained from the theoretical study of the elastic properties of  $(\text{NH}_4)_2\text{BeF}_4$  crystal. The obtained values of  $C_{ij}$  were shown to be in good agreement with previously published experimental data. From the obtained results, Young's modulus  $E$ , Poisson's ratios  $\nu$ , as well as polycrystalline bulk  $B$  and shear  $G$  moduli were calculated for the crystal. The degree of elastic properties anisotropy is shown through the calculated anisotropy coefficients. The 3D surfaces of Young's modulus  $E$  and bulk modulus  $B$  spatial distribution show that Young's modulus has a higher anisotropy than bulk modulus. The greatest anisotropy of Young's modulus is observed for (001) plane.

## Declaration of competing interest

The authors declare that they have no known competing financial interests or personal relationships that could have appeared to influence the work reported in this paper.

## Acknowledgments

The study was performed within the framework of the project 2020.02/0211 of the National Research Foundation of Ukraine “Experimental and theoretical study and prediction of the photoelastic properties of crystalline materials for devices of electromagnetic radiation control”. This work was supported by the PRELUDIUM 15 program of Polish National Science Center (Grant No. 2018/29/N/ST3/02901) and Wrocław Center for Networking and Supercomputing WCSS#10106944.

## References

- [1] A. Ran Lim, H. Hyoun Kim, M. Lee, Characteristic features of the structural properties, phase transitions, and ferroelastic properties in  $\text{LiK}_{1-x}\text{Rb}_x\text{SO}_4$  ( $x = 0, 0.2, \text{ and } 1$ ) crystals, *J. Solid State Chem.* 199 (2013) 96–101, <https://doi.org/10.1016/j.jssc.2012.11.030>.
- [2] B. Chen, T.-H. Liu, H. Jiao, X.-P. Jing, Phase transitions and energy storage properties of some compositions in the  $(1-x)\text{Li}_2\text{SO}_4-x\text{Na}_2\text{SO}_4$  system, *Phase Transitions* 87 (2014) 629–640, <https://doi.org/10.1080/01411594.2013.873436>.
- [3] R.A. Shakhovoy, V. Sarou-Kanian, A. Rakhmatullin, E. Véron, C. Bessada, High-temperature nuclear magnetic resonance study of phase transition kinetics in  $\text{LiNaSO}_4$ , *J. Appl. Phys.* 118 (2015), 243906, <https://doi.org/10.1063/1.4939075>.
- [4] C. Scherf, N.R. Ivanov, S.-J. Chung, T. Hahn, H. Klapper, High-temperature phase transitions and domain structures of  $\text{KLiSO}_4$ : studied by polarisation optics, X-ray topography and liquid–crystal surface decoration, *Zeit. Krist. – Cryst. Mater.* 232 (2017) 415–434, <https://doi.org/10.1515/zkri-2016-2030>.
- [5] A. Sivakumar, S.S.J. Dhas, P. Sivaprakash, A.I. Almansour, R.S. Kumar, N. Arumugam, S. Arumugam, S.A.M.B. Dhas, The switchable phase transition of sodium sulfate crystals activated by shock waves, *New J. Chem.* 45 (2021) 16529–16536, <https://doi.org/10.1039/D1NJ02974F>.
- [6] V.Yo Stadnyk, R.B. Matviiv, R.S. Brezvin, P.A. Shchepanskyi, Z.A. Kogut, On isotropic points in  $\text{K}_2\text{SO}_4$  impurity crystals, *Opt. Spectrosc.* 129 (2021) 227–233, <https://doi.org/10.1134/S0030400X21020144>.
- [7] M.Y. Rudysh, M.G. Brik, O.Y. Khyzhun, A.O. Fedorchuk, I.V. Kityk, P. A. Shchepanskyi, V.Y. Stadnyk, G. Lakshminarayana, R.S. Brezvin, Z. Bak, M. Piasecki, Ionicity and birefringence of  $\alpha\text{-LiNH}_4\text{SO}_4$  crystals: ab initio DFT study, X-ray spectroscopy measurements, *RSC Adv.* 7 (2017) 6889–6901, <https://doi.org/10.1039/C6RA27386F>.
- [8] M.Ya Rudysh, M.G. Brik, V.Yo Stadnyk, R.S. Brezvin, P.A. Shchepanskyi, A. Fedorchuk, O.Y. Khyzhun, I.V. Kityk, M. Piasecki, Ab initio calculations of the electronic structure and specific optical features of  $\beta\text{-LiNH}_4\text{SO}_4$  single crystals, *Phys. B Condens. Matter* 528 (2018) 37–46, <https://doi.org/10.1016/j.physb.2017.10.085>.
- [9] P. Shchepanskyi, O. Kushnir, V. Stadnyk, A. Fedorchuk, M. Rudysh, R. Brezvin, P. Demchenko, A. Krymus, Structure and optical anisotropy of  $\text{K}_{1.75}(\text{NH}_4)_{0.25}\text{SO}_4$  solid solution, *Ukr. J. Phys. Opt.* 18 (2017) 187, <https://doi.org/10.3116/16091833/18/4/187/2017>.
- [10] R.B. Matviiv, M.Ya Rudysh, V.Yo Stadnyk, A.O. Fedorchuk, P.A. Shchepanskyi, R. S. Brezvin, O.Y. Khyzhun, Structure, refractive and electronic properties of  $\text{K}_2\text{SO}_4$ :  $\text{Cu}^{2+}$  (3%) crystals, *Curr. Appl. Phys.* 21 (2021) 80–88, <https://doi.org/10.1016/j.cap.2020.09.015>.
- [11] N.P. Sabalisk, C. Guzmán-Afonso, C. González-Silgo, M.E. Torres, J. Pasán, J. del-Castillo, D. Ramos-Hernández, A. Hernández-Suárez, L. Mestres, Structures and thermal stability of the  $\alpha\text{-LiNH}_4\text{SO}_4$  polytypes doped with  $\text{Er}^{3+}$  and  $\text{Yb}^{3+}$ , *Acta Crystallogr B Struct Sci Cryst Eng Mater* 73 (2017) 122–133, <https://doi.org/10.1107/S2052520616019028>.
- [12] G.L. Myronchuk, G. Lakshminarayana, I.V. Kityk, A.S. Krymus, O.V. Parasyuk, M. Ya Rudysh, P.A. Shchepanskyi, M. Piasecki, Optical absorption, piezoelectric effect and second harmonic generation studies of single crystal  $\text{AgGaGe}_3\text{Se}_7.6\text{Te}_{0.4}$  solid solution, *Appl. Phys. A* 123 (2017) 175, <https://doi.org/10.1007/s00339-017-0823-7>.
- [13] A. Kashuba, H. Ilchuk, R. Petrus, I. Semkiv, O. Bovgyra, M. Kovalenko, V. Dzikovskiy, Optical properties of Al-doped ZnO thin films obtained by the method of high-frequency magnetron sputtering, *Mod. Phys. Lett. B* 35 (2021), 2150189, <https://doi.org/10.1142/S021798492150189X>.
- [14] Y.S. Jain, Infrared spectra of  $(\text{NH}_4)_2\text{BeF}_4$ , *Proc. Indian Acad. Sci.* 87 (1978) 45–48.
- [15] L. Palatinus, M. Amami, S. van Smaalen, Structure of incommensurate ammonium tetrafluoroberyllate studied by structure refinements and the maximum entropy method, *Acta Crystallogr. B* 60 (2004) 127–137, <https://doi.org/10.1107/S0108768104000874>.
- [16] R. Pepinsky, F. Jona, New ferroelectric crystal containing no oxygen, *Phys. Rev.* 105 (1957) 344–345, <https://doi.org/10.1103/PhysRev.105.344>.
- [17] R.C. Srivastava, W.T. Klooster, T.F. Koetzle, Neutron structures of ammonium tetrafluoroberyllate, *Acta Crystallogr. B* 55 (1999) 17–23, <https://doi.org/10.1107/S010876819800737X>.
- [18] N. Yamada, T. Ozawa, T. Ikeda, Disorder of  $\text{BeF}_4$  in the normal phase of  $(\text{NH}_4)_2\text{BeF}_4$ , *J. Phys. Soc. Jpn.* 54 (1985) 1394–1402, <https://doi.org/10.1143/JPSJ.54.1394>.
- [19] M. Iizumi, K. Gesi, Incommensurate phase in  $(\text{ND}_4)_2\text{BeF}_4$ , *Solid State Commun.* 22 (1977) 37–39, [https://doi.org/10.1016/0038-1098\(77\)90938-3](https://doi.org/10.1016/0038-1098(77)90938-3).
- [20] M.O. Romanyuk, V.Yo Stadnyk, The action of mechanical stress and other influences on birefringence inversion of  $\text{LiKSO}_4$  and  $(\text{NH}_4)_2\text{BeF}_4$  crystals, *Ferroelectrics* 192 (1997) 235–241.
- [21] M.O. Romanyuk, M.M. Romanyuk, Inversion of the sign of birefringence and its application in thermometry, *Ferroelectrics* 317 (2005) 57–61, <https://doi.org/10.1080/00150190590963444>.
- [22] M. Tan, A.T. Martin, A.G. Shtukenberg, B. Kahr, Tuning the optical isotropic point of mixed crystals of ethylenediammonium sulfate/selenate, *J. Appl. Crystallogr.* 53 (2020) 53 51–57, <https://doi.org/10.1107/S1600576719015863>.
- [23] Ch Bäumer, D. Berben, K. Buse, H. Hesse, J. Imbrock, Determination of the composition of lithium tantalate crystals by zero-birefringence measurements, *Appl. Phys. Lett.* 82 (2003) 2248–2250, <https://doi.org/10.1063/1.1566100>.
- [24] V.J. Stadnyk, M.O. Romanyuk, Piezooptic properties of  $(\text{NH}_4)_2\text{BeF}_4$  crystals, *Phys. Status Solidi (A) Appl. Res.* 158 (1996) 289–296.
- [25] M.G. Brik, I.V. Kityk, Spectroscopic and crystal field studies of  $(\text{NH}_4)_2\text{BeF}_4$ :  $\text{Co}^{2+}$ , *Solid State Commun.* 143 (2007) 326–330, <https://doi.org/10.1016/j.ssc.2007.05.042>.
- [26] M. Rudysh, B. Horon, P. Shchepanskyi, V. Stadnyk, R. Brezvin, First principles calculation of band structure and physical properties of ferroelectric  $(\text{NH}_4)_2\text{BeF}_4$  crystal, in: 2021 IEEE 12th International Conference on Electronics and Information Technologies, ELIT, 2021, pp. 310–314, <https://doi.org/10.1109/ELIT53502.2021.9501145>.
- [27] S.J. Clark, M.D. Segall, C.J. Pickard, P.J. Hasnip, M.I.J. Probert, K. Refson, M. C. Payne, First principles methods using CASTEP, *Z. für Kristallogr. - Cryst. Mater.* 220 (2005) 567–570, <https://doi.org/10.1524/zkri.220.5.567.65075>.
- [28] P. Hohenberg, W. Kohn, Inhomogeneous electron gas, *Phys. Rev.* 136 (1964) B864–B871, <https://doi.org/10.1103/PhysRev.136.B864>.
- [29] W. Kohn, L.J. Sham, Self-consistent equations including exchange and correlation effects, *Phys. Rev.* 140 (1965) A1133–A1138, <https://doi.org/10.1103/PhysRev.140.A1133>.
- [30] H.J. Monkhorst, J.D. Pack, Special points for Brillouin-zone integrations, *Phys. Rev. B* 13 (1976) 5188–5192, <https://doi.org/10.1103/PhysRevB.13.5188>.
- [31] J.P. Perdew, K. Burke, M. Ernzerhof, Generalized gradient approximation made simple, *Phys. Rev. Lett.* 77 (1996) 3865–3868, <https://doi.org/10.1103/PhysRevLett.77.3865>.
- [32] B.G. Pfrommer, M. Côté, S.G. Louie, M.L. Cohen, Relaxation of crystals with the quasi-Newton method, *J. Comput. Phys.* 131 (1997) 233–240, <https://doi.org/10.1006/jcph.1996.5612>.
- [33] C. Gonzalez Silgo, X. Solans, C. Ruiz Perez, M.L. Martínez Sarrion, L. Mestres, E. H. Bocanegra, Study on the mixed crystals  $[\text{NH}_4]_{2-x}\text{K}_x\text{SO}_4$ , *J. Phys. Condens. Matter* 9 (1997) 2657–2669.
- [34] S. Ahmed, A. Shamah, R. Kamel, Y. Badr, Structural changes of  $(\text{NH}_4)_2\text{SO}_4$  crystals, *Phys. Status Solidi A* (1987), <https://doi.org/10.1002/PSSA.2210990116>.
- [35] A.O. Fedorchuk, O.V. Parasyuk, I.V. Kityk, Second anion coordination for wurtzite and sphalerite chalcogenide derivatives as a tool for the description of anion sublattice, *Mater. Chem. Phys.* 139 (2013) 92–99, <https://doi.org/10.1016/j.matchemphys.2012.12.058>.
- [36] A.O. Fedorchuk, M.F. Fedyna, I.V. Kityk, Nearest Coordination Environment of Atoms in Inorganic Compound Structures, *Rodovid, Chemivisti*, 2013.
- [37] B. Andriyevskiy, M. Jaskólski, V.Y. Stadnyk, M.O. Romanyuk, Z.O. Kashuba, M. M. Romanyuk, Electronic band structure and influence of uniaxial stresses on the properties of  $\text{K}_2\text{SO}_4$  crystal: ab initio study, *Comput. Mater. Sci.* 79 (2013) 442–447, <https://doi.org/10.1016/j.commatsci.2013.06.048>.
- [38] M. Chrunik, A. Majchrowski, K. Ozga, M.Ya Rudysh, I.V. Kityk, A.O. Fedorchuk, V. Yo Stadnyk, M. Piasecki, Significant photoinduced increment of reflectivity coefficient in  $\text{LiNa}_3\text{Mo}_9\text{O}_{30}$ , *Curr. Appl. Phys.* 17 (2017) 1100–1107, <https://doi.org/10.1016/j.cap.2017.05.001>.
- [39] M.Ya Rudysh, P.A. Shchepanskyi, A.O. Fedorchuk, M.G. Brik, C.-G. Ma, G. L. Myronchuk, M. Piasecki, First-principles analysis of physical properties anisotropy for the  $\text{Ag}_2\text{SiS}_3$  chalcogenide semiconductor, *J. Alloys Compd.* 826 (2020), 154232, <https://doi.org/10.1016/j.jallcom.2020.154232>.
- [40] P.A. Shchepanskyi, V.Yo Stadnyk, M.Ya Rudysh, R.S. Brezvin, B.V. Andrievskii, Energy band structure and optical properties of  $\text{LiNaSO}_4$  crystals, *Opt. Spectrosc.* 125 (2018) 353–357, <https://doi.org/10.1134/S0030400X18090217>.
- [41] M.D. Segall, P.J.D. Lindan, M.J. Probert, C.J. Pickard, P.J. Hasnip, S.J. Clark, M. C. Payne, First-principles simulation: ideas, illustrations and the CASTEP code, *J. Phys. Condens. Matter* 14 (2002) 2717–2744, <https://doi.org/10.1088/0953-8984/14/11/301>.
- [42] D. Sanchez-Portal, E. Artacho, J.M. Soler, Projection of plane-wave calculations into atomic orbitals, *Solid State Commun.* 95 (1995) 685–690, [https://doi.org/10.1016/0038-1098\(95\)00341-X](https://doi.org/10.1016/0038-1098(95)00341-X).
- [43] M. Fox, *Optical Properties of Solids*, Oxford University Press, Oxford, 2001.
- [44] M. Dressel, B. Gompf, D. Faltermeier, A.K. Tripathi, J. Pflaum, M. Schubert, Kramers-Kronig-consistent optical functions of anisotropic crystals: generalized spectroscopic ellipsometry on pentacene, *Opt Express* 16 (2008) 19770–19778.
- [45] A. Majchrowski, M. Chrunik, M. Rudysh, M. Piasecki, K. Ozga, G. Lakshminarayana, I.V. Kityk,  $\text{Bi}_2\text{TeO}_5$ : electronic structure, optical properties

- and photoinduced phenomena, *J. Mater. Sci.* 53 (2018) 1217–1226, [10.1007/s10853-017-1554-z](https://doi.org/10.1007/s10853-017-1554-z).
- [46] Z. Wu, E. Zhao, H. Xiang, X. Hao, X. Liu, J. Meng, Crystal structures and elastic properties of superhard IrN<sub>0</sub> and IrN<sub>3</sub> from first principles, *Phys. Rev. B* 76 (2007), 054115, <https://doi.org/10.1103/PhysRevB.76.054115>.
- [47] A. Garg, R.C. Srivastava, Characteristic Debye temperature of ammonium fluoroberyllate, (NH<sub>4</sub>)<sub>2</sub>BeF<sub>4</sub>, *Acta Crystallogr. A* 38 (1982) 388–390, <https://doi.org/10.1107/S0567739482000783>.
- [48] B. Andriyevsky, K. Doll, M. Jansen, First principles study of structural stability, electronic and related properties of (NH<sub>4</sub>)<sub>2</sub>SO<sub>4</sub>, *J. Phys. Chem. Solid.* 71 (2010) 357, <https://doi.org/10.1016/j.jpcs.2009.12.090>.
- [49] Y. Luspin, G. Hauret, Etude de l'effet Brillouin, a temperature ordinaire, dans le sulfate d'ammonium, *Compt. Rend. Hebd. Seances Acad. Sci. (Paris). B* (1974) 995.